Version: Post-print

Flexural and Shear Characteristics of Bio-Based Sandwich Beams Made of Hollow and Foam-Filled Paper Honeycomb Cores and Flax Fiber Composite Skins

Yuchen Fu and Pedram Sadeghian[1]

Department of Civil and Resource Engineering, Dalhousie University, 1360 Barrington

Street, Halifax, NS, B3H 4R2, Canada

ABSTRACT

In this paper, bio-based sandwich panels made of fiber-reinforced polymer (FRP) skins and two types of paper honeycomb core (namely, hollow and foam-filled) with three different thicknesses (namely, 6 mm, 12 mm, and 25 mm) were studied. Flax FRP composites made of a unidirectional plant-based flax fabric and bio-based epoxy resin (30% bio content) were used for the skins. The panels were cut into a total of 36 sandwich beam specimens with the width of 50 mm and tested under four-point bending with two span configurations to characterize the flexural and shear stiffness of the panels. The specimens with foam-filled paper honeycomb cores showed a higher load capacity than those with hollow honeycomb, however their stiffnesses were not fundamentally different. Major non-linearity was observed in the load-deflection and load-strain behavior of the specimens. An analytical model was successfully developed based on the non-linearity of the skins in tension/compression and the core in shear to predict the non-linear behavior of the specimens. A parametric study was performed on

---

[1] Corresponding Author: Assistant Professor and Canada Research Chair in Sustainable Infrastructure, Pedram.Sadeghian@dal.ca

different geometrical parameters and it was shown that contribution and bending and shear changes and it can be engineered to achieve desirable strength and stiffness. Overall, the bio-based sandwich panels can be used for interior walls, doors, and furniture in building application with much less impact on the environment in comparison with their synthetic counterparts.

1. INTRODUCTION

Sandwich composites are efficient systems with high performance at low cost and low weight. The skins of a sandwich beam resist the tensile and compressive stresses under flexure, while lightweight and low-density core provides shear stress resistance and maintains a distance between skins resulting in a higher moment of inertia. Moreover, the core prevents heat flux infiltration, so it provides insulation for the system. Honeycomb structures have been extensively studied for the core of sandwich composites [1][2][3][4][5][6]. On the other hand, sandwich composites with fiber-reinforced polymer (FRP) skins made of synthetic fibers (such as carbon, glass, basalt, and etc.) have been practices for a long time [7][8][9]. Recently, it has been shown that plant-based fibers (such as flax, hemp, jute, and etc.) can be more efficient for cases that skin strength is not critical [10][11][12]. Plant-based fibers are considered as prospective substitutes to synthetic fibers due to the relatively large quantity, low cost of raw material, low density, high specific properties, and positive environmental profile [13][14][15]. Using bio-based polymer with flax fibers makes flax FRPs even more environmentally friendly

than FRPs made of synthetic polymers [16][17][18].

In addition to skin materials, many different light-weight, low-density, and low-strength core materials have been developed to be used in the form of foams [19][20], honeycombs [21][22], and woven fabrics [23][24]. Hollow honeycomb cores have been widely applied to sandwich composites due to their light-weight, high performance to cost ratio, excellent stiffness, and good bonding surface [25][26][27]. Sandwich composites with honeycomb cores have substantial empty space within the core cells, which can be filled with foams. Foam-filled honeycomb cores can provide the combined advantages of traditional foam cores and hollow honeycomb cores resulting in higher shear strength and stiffness plus cell stability [28][29][30]. Recently, multiple studies have been conducted on the impact behavior of sandwich composites made of foam-filled metallic honeycomb cores [31][32][33].

Paper honeycomb cores are products with honeycomb structure and cell walls made of paper-based materials. Due to its lightweight, high strength, and favorable cushioning properties, paper honeycomb products have been widely used in packaging industry and others such as aviation, furniture, and building industries [34][35][36]. Besides, paper is an environmentally friendly material with very high recyclability potential. Numerous studies have been conducted on sandwich composites made of bio-based components. A variety of bio-based core materials including corrugated cardboard [37][38][39][40], hollow paper honeycomb [34][36][41], and cork[26][42][43][44] have been studies in the past. Also, natural fibers and bio-based polymers [45][46][47][48] have been incorporated into skins of sandwich structures. However, the effects of filling foam on the behavior and failure of sandwich panels

made of a paper honeycomb core and flax FRP composite skins considering the non-linearity of both the skins and core have not been studied.

In this study, flax FRP skins and paper honeycomb (hollow and foam-filled) were combined to manufacture sandwich beam specimens. High performance unidirectional flax fabric is a general material used in automotive, sporting goods and decorative application. Therefore, the flax is environmentally friendly and has fewer health and safety concerns than traditional materials. Paper honeycomb, as mentioned earlier, is a recyclable and reusable material. The whole sandwich beam specimens can be considered as a green construction material. This paper evaluates the flexural and shear characteristics of a novel composition of paper honeycomb cores and flax FRP skins to achieve a more environmentally friendly design than conventional systems for sandwich structures.

2. EXPRIMENTAL PROGRAM

This section presents the details of test matrix, material properties, specimen fabrication, and test setup and instrumentation.

2.1. Test Matrix

A total of 36 flax FRP and paper honeycomb core sandwich beams with the width of 50 mm were manufactured and tested under four-point bending. All specimens were fabricated using one-layer flax FRP skin on each sides of the core. The variables of the test were thickness and type of the cores. Three core thicknesses of 6 mm, 12 mm and 25 mm as well as two core types of hollow and foam-filled were used. Two beams spans were considered for each configuration of core type and thickness. As shown in Table 1, a total of 12 cases were considered. Note that

three identical specimens per case were manufactured and tested. A specimen identification (ID) with the format of AX-Y is used to identify each specimen. "A" indicates the core type (H: hollow and F: foam-filled), "X" identifies the core thickness in mm, and "Y" stands for span in mm. For example, the specimen F6-300 was manufactured by foam-filled core with the thickness of 6 mm and tested with the span of 300 mm. The three core thicknesses were selected based on the panel thicknesses available to the authors. The two span lengths were selected based on the limitation of testing fixture and travel length of displacement gauges. The span of 300 mm was selected as the base and the second span was selected to ensure the specimen can reach to a failure. The second span also enabled the authors to obtain flexural and shear stiffness of the specimens, which will be discussed later in this paper.

Table 1. Test Matrix.

Case #	Specimen group ID	Core type	Core nominal thickness (mm)	Span (mm)	Total thickness (mm)	Core actual thickness (mm)	Shear span/thickness ratio	Number of specimens
1	H6-200	H	6	200	9.1	8.1	9	3
2	H6-300	H	6	300	9.1	8.1	13	3
3	F6-200	F	6	200	8.2	7.2	10	3
4	F6-300	F	6	300	8.2	7.2	15	3
5	H12-300	H	12	300	15.5	14.5	8	3
6	H12-400	H	12	400	15.5	14.5	11	3
7	F12-300	F	12	300	15.3	14.3	8	3
8	F12-350	F	12	350	15.3	14.3	9	3
9	H25-300	H	25	300	28.5	27.5	4	3
10	H25-400	H	25	400	28.5	27.5	6	3
11	F25-300	F	25	300	28.5	27.5	4	3
12	F25-400	F	25	400	28.5	27.5	6	3
Total								36

Note: H=Hollow; F= Foam-filled

2.2. Material Properties

A honeycomb core with regular hexagonal cells made of a phenolic treated kraft paper was used in this study as shown in Figure 1. The paper honeycomb cores were provided in the form of hollow cell and foam-filled cell panels with the dimension of 610 mm x 610 mm and three of thicknesses of 6 mm, 12 mm and 25 mm. The average bulk density of the hollow and foam-filled cores was measured as 40 kg/m^3 and 114 kg/m^3, respectively. The average cell size of the honeycomb core was also measured as presented in Fig. 1. The 25-mm thick foam-filled core had the compressive, flexural, and shear strength of 3013 kPa (437 psi), 692 kPa (100 psi) at 5% strain, and 1076 kPa (156 psi), respectively, per the manufacturer (RhinoKore Composites Solutions Inc., Armstrong, BC, Canada). Polyurethane foam with the bulk density of 5 pcf (80 kg/m^3) was used by the manufacturer to fill the paper honeycombs. The properties of the foam and other cores were not provided by the manufacturer. The most important parameter is the shear modulus of the core materials, which will be also determined through the current experimental study.
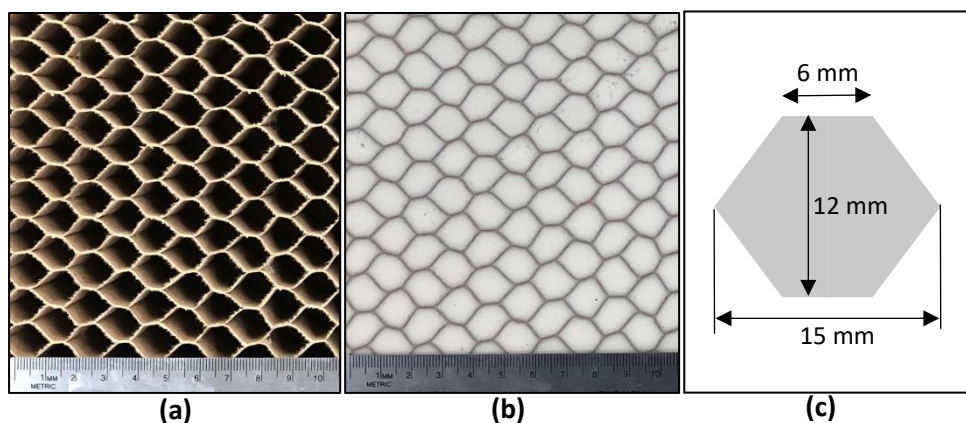

Figure 1. Paper honeycomb cores: (a) hollow core; (b) foam-filled core; and (c) geometry of a typical honeycomb cell.

For flax FRP skins, a unidirectional flax fabric was used with a reported weight of 275 g/m^2 and density of 1.28 g/cm^3 reported by manufacturer (Composites Evolution, Chesterfield, UK). A bio-based epoxy resin (30% bio content) with a fast setting hardener was used to make the flax FRP skins. Epoxy and hardener are mixed at the ratio of 100 to 43 by weight, and it had a reported fully cure time of 7 days. The mechanical properties were determined as tensile strength, modulus and elongation of 53.23 MPa, 2.65 GPa, and 6% reported by the manufacturer (Entropy Resins, Hayward, USA). The flax FRP with a ply thickness of 0.5 mm was previously reported [49] to have a non-linear behavior in tension. The tensile strength, initial modulus, and ultimate strain were reported to be 198 MPa, 17.09 GPa, 0.0153 mm/mm, respectively.

2.3. Specimen Fabrication

Initially, sandwich panels with the size of the honeycomb core (i.e., 610 mm x 610 mm) were manufactured and then were cut into difference specific beam size. Significant steps are shown in Figure 2. First, two pieces of square wooden board with the same size of the honeycomb core sheet were prepared, and they were sanded by sandpaper and cleaned to have flat surfaces. One of square wooden boards was places on a flat table and covered by a wax paper. Flax fabric was also cut to cover the surface of the honeycomb core sheet. Then, the epoxy and hardener were mixed per manufacturer's guideline, and a layer of resin was spread on the wax paper using brush and scraper. Then, the flax fabric was placed on the resin coated surface. Additional resin was applied on the flax fabric to saturate it. A scraper was used to spread the resin and remove any excess resin. Then, the honeycomb core was placed on saturated flax fabric. The

longitudinal direction of the honeycomb core was placed parallel to the fiber direction of the unidirectional flax fabric. Finally, a weighted flat wooden board was placed on the top face of the core to set for a minimum of 24 hours. Next day, the same steps were repeated for making the other skin of the sandwich panel. After minimum of seven days curing at room temperature, the panels were cut into 50-mm wide strips parallel to the longitudinal direction of the flax FRP skins. Then the strips were cut into required length per Table 1. All specimens were cut 50 mm longer than the testing span to provide 25 mm overhang at each side.
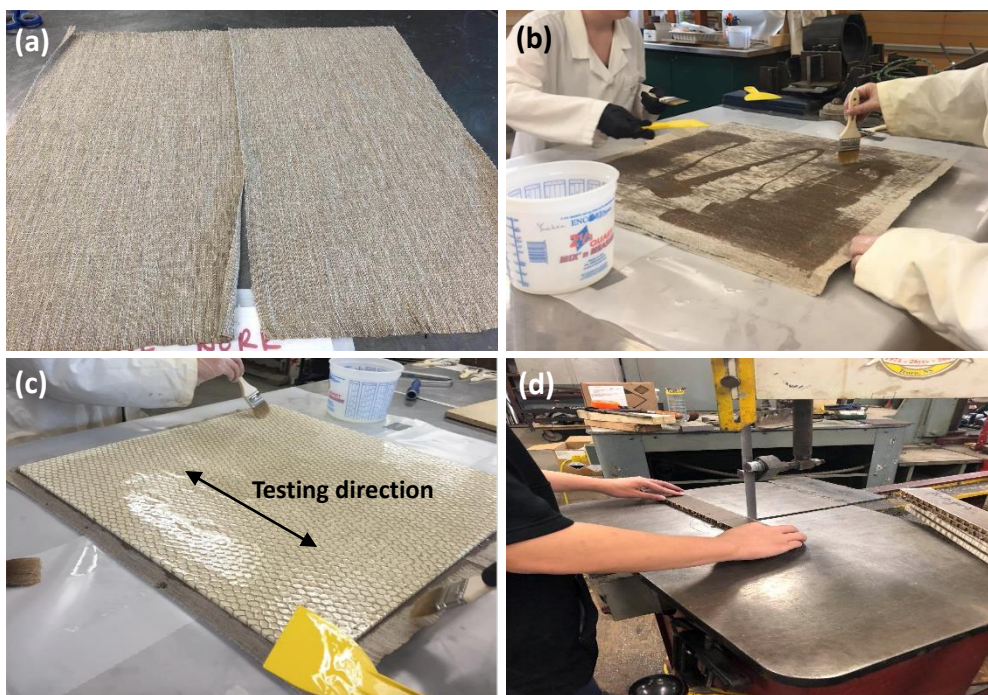

Figure 2. Specimen fabrication: (a) flax fabric prepared; (b) saturating flax fabric; (c) placing resin on core; and (d) cutting cured panels.

2.4. Test Setup and Instrumentation

All specimens were tested under four-point bending with a loading span proportional to the supporting span in this study. According to ASTM D7250 [51], the loading span L was decided to be equal to (2/11) of supporting span S. A schematic of the four-point bending setup is shown

in Figure 3, and P is the total load. In terms of instrumentation, a strain gauge was applied centered along the longitudinal direction on each side of the sandwich beam at the mid-span to measure the tensile strain at the bottom and compression strain on the top. Besides, two linear potentiometers (LPs) were installed at mid-span of specimen to measure the deflection. All tests were completed using a universal testing machines and were displacement controlled using a fixed rate of 2 mm/min. The data (load, deflection, and strains) was collected every 0.1 second for data processing.
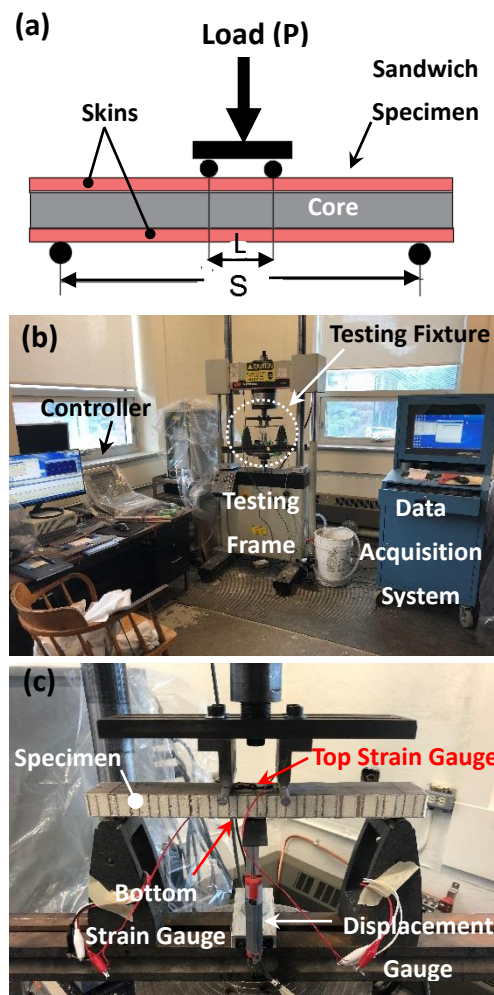

Figure 3. Test setup and instrumentation: (a) four-point bending schematic; (b) testing machine and data acquisition system; and (c) specimen ready for testing.

3. EXPERIMENTAL RESULTS AND DISCUSSIONS

This section presents the details of the failure modes, the load-deflection and load-strain, behaviors, and the stiffness calculations based on the moment-curvature and ASTM methods. A summary of the test results is shown in Table 2.

Table 2. Summary of test results.

Case #	Specimen Group ID	Peak load (N)		Initial stiffness, K (kN/m)		Def. at Peak (mm)		Failure Modes (see Note 2)
		AVG	SD	AVG	SD	AVG	SD	
1	H6-200	579	69	59.9	3.5	17.32	1.72	Indentation (3)
2	H6-300	465	56	23.4	0.8	36.28	6.03	Not failed (2) / Dimpling (1)
3	F6-200	583	80	55.6	1.8	18.78	4.42	Wrinkling (2) / Indentation (1)
4	F6-300	344	26	19.1	1.1	34.12	3.61	Not failed (2) / Wrinkling (1)
5	H12-300	764	90	67.4	4.6	19.16	0.50	Dimpling (1) / Indentation (2)
6	H12-400	514	15	31.5	0.1	34.04	1.48	Dimpling (1) / Indentation (2)
7	F12-300	1140	39	73.6	3.0	23.45	2.29	Tensile rupture (3)
8	F12-350	732	117	49.7	3.8	30.32	6.85	Wrinkling (3)
9	H25-300	873	130	222.8	15.4	6.68	0.86	Indentation (2) / Core shear (1)
10	H25-400	887	298	113.3	3.1	14.64	3.20	Indentation (2) / Core shear (1)
11	F25-300	1600	239	252.5	10.6	10.06	1.85	Wrinkling/Core shear/Indentation
12	F25-400	1391	131	122.9	12.5	20.72	0.67	Tensile rupture/Indentation/Core shear

Note 1: AVG = average; and SD = standard deviation.

Note 2: The numbers in the brackets indicate the number of specimens (out of 3 identical specimens) with identical failure mode.

3.2. Failure Modes

A total of five failure modes were observed during the test, namely (a) tensile rupture, (b) indentation, (c) core shear, (d) wrinkling, and (e) dimpling as shown in Figure 4. The dimpling failure is the local buckling of the compression skin between the walls of a hollow honeycomb cell of the core. Table 2 presents the failure modes of each group of specimens. As shown in the table, for some group of specimens, more than one failure mode was observed by testing

three identical specimens. The numbers in the brackets in the failure mode column of the table indicate the number of the specimens with identical failure mode. This means that the load corresponding to some of failure modes are very close to each other causing to switch from one failure mode to another one due to minor differences in geometry and location of honeycomb cells.
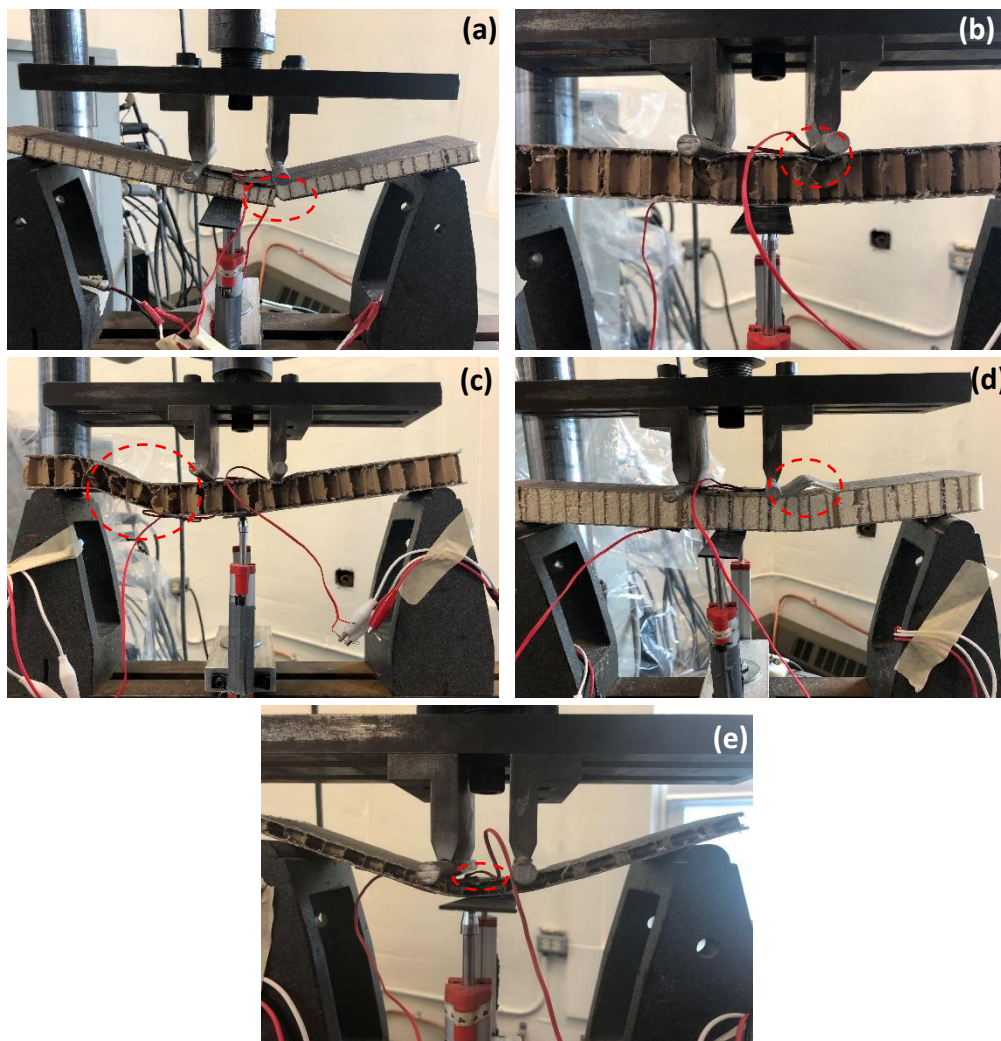

Figure 4. Typical failure modes: (a) tensile rupture; (b) indentation; (c) core shear; (d) wrinkling; and (e) dimpling.

For the specimens with hollow core, the failure modes of short and long spans were not changed. However, for the specimens with foam-filled core, different failure modes were

obtained in different span. Moreover, the filling foam significantly changed the failure mode of the specimens with 12- and 25-mm thick honeycomb core. This can be explained with the lateral support provided by the filling foam for the core cells and compressive skin. The specimens with 12-mm thick core filled with foam showed consistent failure mode in comparison with their counterparts.

3.3. Load-Deflection Behavior

The deflection of each specimen was calculated based on averaging two LPs placed at the mid-span and on the bottom skin of each specimen. As shown in Figure 5, the load-deflection behavior of the specimens with foam-filled core were slightly stiffer that their counterparts with hollow core; however, the specimens with foam-filled core took significantly higher load than the hollow specimens (except 6-mm core specimens). The initial stiffness of each specimen was calculated based on the initial slope of load-deflection curve.
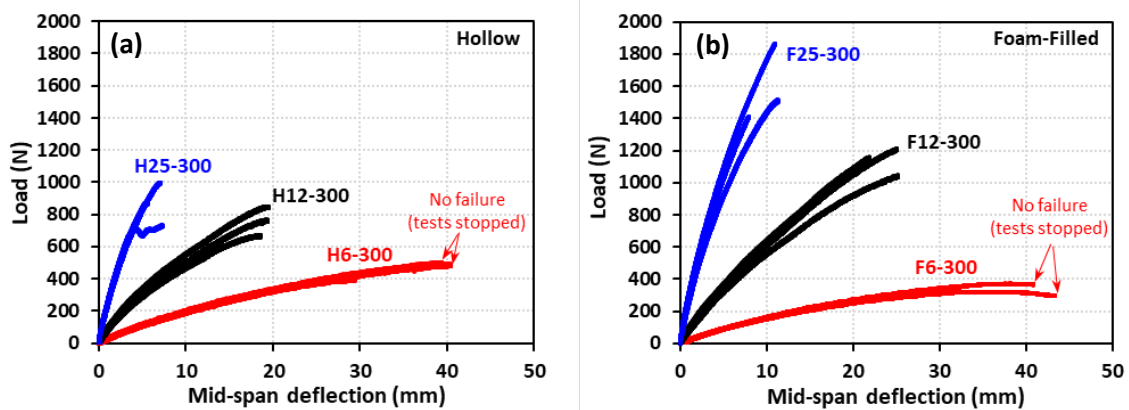

Figure 5. Load-deflection behaivor of specimens with: (a) hollow; and (b) foam-filled paper honeycomb core.

Because of the non-linear behavior of the specimens, the initial stiffness was calculated by truncating the non-linear tail of the curve until the diagram was close to a line representing the

initial stiffness of the specimen. The test results of initial stiffness were shown in the Table 2 and will be used in the analytical section to calculate flexural and shear stiffness. Each value presented in the table is the average of three identical specimens. The standard deviation of each parameter is also provided in the table. Overall, higher values of stiffness were obtained when the core became thicker. For 300 mm spans, the initial stiffness of the specimens with 25- and 12-mm thick foam-filled core were 13 and 9% higher than that of their counterparts with hollow core, respectively. For 200- and 300-mm spans, the initial stiffness of the specimens with 6-mm thick foam-filled core were averagely 13% less that of their counterparts with hollow core. This can be explained based on the fact that the 6-mm thick foam-filled core was slightly (about 1 mm) thinner that of its hollow counterpart as presented in Table 1.

The average peak load of each group of specimens along with corresponding standard deviation are also presented in Table 2. For 300 mm spans, the peak load of the specimens with 25- and 12-mm thick foam-filled core were 83 and 49% higher than that of their counterparts with hollow core, respectively. This indicates that the filling foam prevented failures triggered with the lack of stability of hollow cell walls. For 200- and 300-mm spans, the peak load of the specimens with 6-mm thick foam-filled core were averagely 13% less that of their counterparts with hollow core, which can be explained as same as the initial stiffness. Overall, the foam-filling increased the load capacity of the hollow core specimens significantly. The non-linearity of the load-deflection behavior of the test specimens is significant, which will be discussed later in the analytical section.

3.4. Load-Strain Behavior

Two strain gauges were applied longitudinally on the center of each side of each specimen at mid-span, and strain values were recorded at every load step. The load-strain curves of the test specimens with 300 mm span are shown in Figure 6. As shown in the figure, when the load was increasing, the top strain was decreasing caused by compression resulting in negative number, and the bottom strain was going up caused by tension resulting in positive value. As seen, at the same value of strain, a higher load was obtained for the specimens with thicker core indication a higher stiffens as expected. Also, the ultimate strain of the hollow core specimens was higher for the specimens with thinner core. However, the ultimate strain of the foam-filled core specimens did not change significantly by changing the core thickness. This indicates that the specimens with thicker foam-filled core were able to utilize the capacity of the skins more than the specimens with hollow cores.
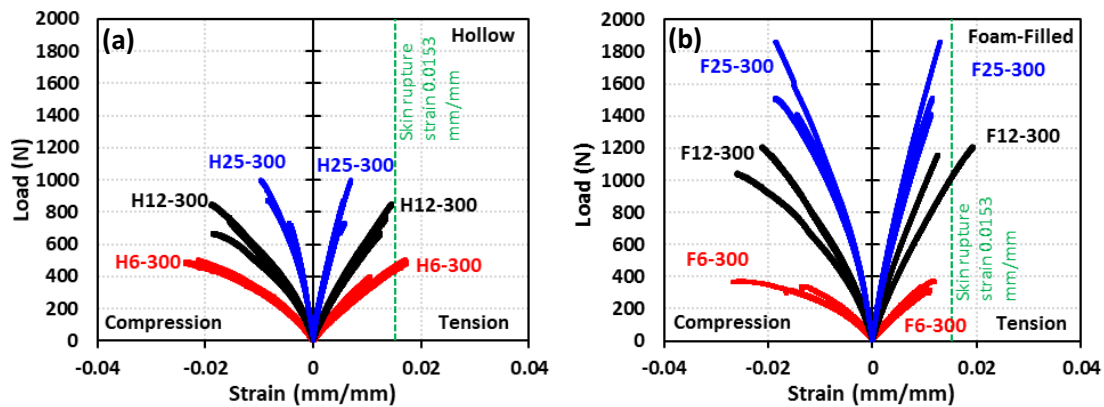

Figure 6. Load-strain behavior of specimens with: (a) hollow; and (b) foam-filled paper honeycomb core.

Figure 6 also shows a non-linear load-strain behavior indicating the source of non-linearity is not only the core and the flax FRP skins of the sandwich specimens also contributed in the non-linear behavior. This needs to be further verified in the analytical section. The maximum

tensile strain of the specimens is typically less than the rupture strain of the skin in tension (i.e., 0.0153 mm/mm), which shows majority of the specimens did not reach to the tensile rupture of the skin. As shown in Figure 6, the curves related to the specimen group F12-300 show a clear intersection with the skin rupture strain on 0.0153 mm/mm, which is compatible with its failure mode (i.e. tensile rupture) observed during the tests. The maximum tensile strain of the specimens with 6- and 12-mm thick hollow core were close to, but mainly less than the skin rupture strain on 0.0153 mm/mm, however they were mainly failed by indentation or dimpling. This might be related to localized high strains due to indentation or dimpling of the skins at the mid-span of those specimens. A finite element modeling of those specimens is recommended to provide a better understanding of the localized strain distribution of the unsupported skin between cell walls of the hollow honeycombs.

3.5. Flexural Stiffness Based on Moment-Curvature Behavior

The moment was calculated for mid-span of the specimens and the curvature was calculated based on the values of strain from two strain gauges applied on the center of each sides of the specimens. The values of moment and curvature were calculated for each load level. The moment-curvature curves of the specimens with 300 mm span are shown in Figure 7. The average moment capacity of 47 N-m (940 N-m/m) obtained from H12-300 specimens (total thickness of 14.5 mm and width of 45 mm) was significantly less than the moment capacity of 64 N-m (1430 N-m/m) of a group of specimens made of aluminum honeycomb core and facings (total thickness of 11 mm and core bulk density of 130 kg/m^3) tested recently by Palomba et al. [50]. This indicates that the hollow paper honeycombs considered in this study were not as

strong as their counterparts made of aluminum, however filling the paper honeycomb cells with the foam increased the moment capacity to an average of 70 N-m (1400 N-m/m) for F12-300 specimens, which is comparable to the aluminum sandwich specimens. It should be highlighted that the filling foam increased the average bulk density of the hollow paper from 40 kg/m^3 to 114 kg/m^3, which is comparable to the bulk density of 130 kg/m^3 for the aluminum honeycomb core.
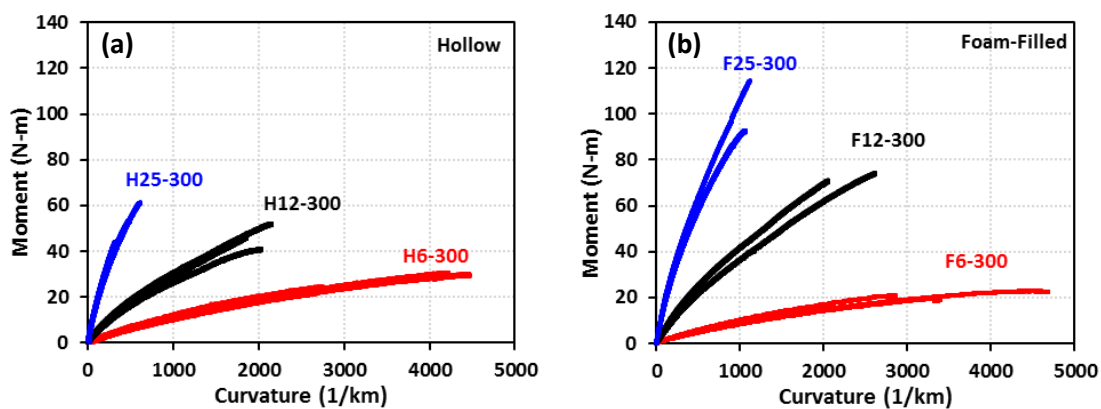

Figure 7. Moment-curvature behavior of specimens with: (a) hollow; and (b) foam-filled paper honeycomb core.

The slope of the moment-curvature represents the flexural stiffness D of each specimen. As expected, a higher flexural stiffness is visible for the specimens with thicker cores. A different moment-curvature behavior was not observed between two types of the core. However, the specimens with foam-filled core took larger moment before failure. Besides, the flexural stiffness of each specimen was calculated based on the initial linear region of each curve and presented in Table 3. The flexural stiffness of each configuration of core was obtained by averaging the flexural stiffness of each span group of specimens. Overall, the results indicate that the flexural stiffness of the foam-filled core specimens is slightly higher

than that of the hollow core specimens. This is logical as the core does not contribute in the flexural stuffiness significantly. The core affects the shear stiffness overall deflection and initial stiffness K of the specimens as presented in Table 2. The flexural stiffness obtained based on the moment-curvature method in this section is compared against that of based on the ASTM method in the next section.

Table 3. Summary of flexural and shear stiffness of the test specimens

Sandwich core type		Flexural stiffness, D (N-m²)				D_{ASTM} to D_{MC} ratio	Shear stiffness, U (kN)	Shear modulus, G (MPa)	Average G (MPa)
		ASTM method, D_{ASTM}	MC method, D_{MC}						
			Span 1	Span 2	Average				
Hollow	H6	16.84	10.81	13.29	12.05	1.40	5.64	11.90	19.62
	H12	46.49	43.24	34.31	38.78	1.20	18.59	22.92	
	H25	195.72	172.08	161.69	166.89	1.17	35.10	24.05	
Foam-filled	F6	11.74	10.55	10.88	10.72	1.10	9.19	21.37	26.18
	F12	52.94	53.58	45.65	49.62	1.07	17.77	22.33	
	F25	194.72	176.24	175.05	175.65	1.11	50.87	34.85	
Average						1.17			

Note: MC = moment-curvature method

3.6. Flexural Stiffness Based on ASTM Method

According to ASTM D7250 [51], the flexural stiffness D and the shear stiffness U can be calculated based on the initial stiffness K from two different spans by equation:

$$K_i = \left(\frac{2S_i^3 - 3S_iL_i^2 + L_i^3}{96D} + \frac{S_i - L_i}{4U} \right)^{-1} \tag{1}$$

where S is the supporting length in mm, and L is the loading span in mm. Parameters K, S, and L from two spans were used to establish equation system of two equations and two unknowns of D and U. The subscript $i = 1$ denotes the parameters to the short-span specimens, and $i = 2$

to the long-span specimens. The initial stiffness K of each specimens was taken from Table 2 and then D and U were calculated for each sandwich configuration by solving the equation system of two unknowns and two equations presented in Equation 1. The results are presented in Table 3 and labeled as ASTM method. The flexural stiffness values obtained from the moment-curvature method for each span are also presented in Table 3. The ratio of the flexural based on the ASTM method to the average of moment-curvature (MC) method is also presented in Table 3. Overall, the ASTM method gives the flexural stiffness of the sandwich specimens 17% higher than that of based on the MC method.

3.7. Shear Modulus

Based on the ASTM method, the shear stiffness U of each sandwich type was also calculated and presented in Table 3. Based on that, the shear modulus G of each core type can be obtained as follows:

$$G = \frac{U(h - 2t)}{b(h - t)^2} \tag{2}$$

where h is the height of the specimen, t is the thickness of the skin, and b is the width of the specimen. The average dimensions of each specimen group were used, and the shear modulus G of each core type was calculated and presented in Table 3. The average shear modulus of the hollow and foam-filled honeycomb cores used in this study are obtained 19.6 and 26.2 MPa, respectively. The shear modulus 19.6 MPa for the hollow paper honeycomb core is compatible with the range of 18 MPa to 22 MPa reported by Chen and Yan [36] based on a finite element modeling of hollow paper honeycomb core with the cell size of 12.7 mm and the core height to face thickness ratio (i.e. shelling ratio) of 4 and more. The shelling ratio of the specimens

tested in the current study ranges from 14 to 55. It should be noted that the actual thickness of the cores used in this study are different than the nominal values used to name the specimens (see Table 1). The shear modulus results are implemented in the next section to predict the shear deformation of the sandwich specimens.

4. ANALYTICAL STUDY

In this section, an analytical study is presented to predict the non-linear behavior of the sandwich specimens. Also, the initial stiffness and peak load of the test specimens are predicted based on classic equations obtained from the literature.

4.1. Non-Linear Behavior

In the experimental section, it was shown that both the load-deflection and load-strain behavior of the sandwich beams were non-linear. It was concluded the source of the non-linearity is both the flax FRP skins and the paper honeycomb core. In this section, a non-linear analytical model is presented to predict the load-deflection behavior of the sandwich specimens tested in the experimental program. The analytical model utilizes the non-linearity of both skin and core materials to calculate the flexural and shear deformations.

4.1.1. Assumptions

In this study, parabolic stress-strain curves for both flax FRPs (in tension and compression) and paper honeycomb core (in shear) are implemented. The parabolic stress-strain curves were previously proposed [37][52] and verified against independent test data. Also, the stress-strain curve of the skins is assumed to be the same in tension and compression. Moreover, it is assumed that the axial strain to vary linearly over the cross-section of the beam according to

the Euler-Bernoulli beam theory. This assumption will be further discussed at the end of this section. Based on a cross-sectional analysis and the assumption of linear and symmetric strain profile with respect to the centroidal axis, the following iterative procedure is implemented to obtain the non-linear load-strain and load-deflection behavior of the test specimens.

4.1.2. Iterative analysis

Based on the non-linearity of the skin and core, an iterative analysis is used to calculate the normal stress σ of the skin under the bending moment M and the shear stress τ of the core under the shear force V at any given load step j as follows:

$$\sigma_j = \frac{M_j}{dbt} \tag{3}$$

$$\tau_j = \frac{V_j c}{bd^2} \tag{4}$$

where d is center-to-center distance of the skins, t is the skin thickness, c is the core thickness, and b is the width of the specimen. Then, the skin normal strain ε and the core shear strain γ is calculated based on the non-linear stress-strain curves of the skin and the core as follows:

$$\varepsilon_j = \frac{1}{\sigma_u^2}\left(\varepsilon_u - \frac{\sigma_u}{E_o}\right)\sigma_j^2 + \frac{1}{E_o}\sigma_j \tag{5}$$

$$\gamma_j = \frac{1}{\tau_u^2}\left(\gamma_u - \frac{\tau_u}{G_o}\right)\tau_j^2 + \frac{1}{G_o}\tau_j \tag{6}$$

where σ_u is the rupture stress of the skin, ε_u is the rupture strain of the skin, E_o is the initial elastic modulus of the skin, τ_u is the shear strength of the core, γ_u is the ultimate shear strain of the core, and G_o is the initial modulus of the core. Then, the secant elastic modulus of the skin E_{sec} and the secant shear modulus the core G_{sec} are obtained by dividing the normal and shear stress to their corresponding strains at any given load step. Subsequently, the secant flexural stiffness D_{sec} and the secant shear stiffness U_{sec} are calculated at any given load step as follows:

$$D_{sec_j} = E_{sec_j} \left(\frac{bt^3}{6} + \frac{btd^2}{2} \right) \tag{7}$$

$$U_{sec_j} = G_{sec_j} \frac{bd^2}{c} \tag{8}$$

where b is the width of specimen, t is the thickness of skin, d is the distance of center lines of skins, and c is thickness of core. Ultimately, the bending and shear deflection of the sandwich beam are obtained based on the secant moduli at the corresponding load step. The procedure is continued until the sandwich beam reaches to its peak load. The total deflection Δ_j at the load step j under the load P_j is obtained as follows:

$$\Delta_j = \frac{P_j(2S^3 - 3SL^2 + L^3)}{96D_{sec_j}} + \frac{P_j(S - L)}{4U_{sec_j}} \tag{9}$$

where S is the support span length, L is the load span length.

4.1.3. Model verification

Figure 8 compares the performance of the analytical model predicting load-strain and load-deflection behaviors of the test specimen group F25-300 and H25-300. Also, a linear model based on initial elastic modulus of flax FRPs are presented in the figure. The initial slope of the load-deflection curve is also used to predict the stiffness of the test specimens, which is discussed at the end of this section. As shown in Figure 8(a), the predicted strain of the top skin (in compression) deviated from experimental strain at higher loads. This means that the top skin of the specimen experienced more strain than that of the model. Lower modulus of FRP skin in compression than that of in tension and/or a slight indentation of top skin due to loading rollers might be the source(s) of the deviation. The damage behavior of composite materials in compression is more complicated than that of in tension. There is a possibility of micro

buckling of fibers in compression and premature buckling of unsupported or poorly supported

skin due to improper bond to the honeycomb core. More in-depth analysis is needed to capture

the actual compressive strain of the top skin and determine the location of actual neutral axis

consequently. This is beyond of the scope of the current paper and needs to be investigated in

the future. As shown in Figure 8(b), the load-deflection curve obtained from the non-linear

model is slightly stiffer than that of the experimental at higher loads. This might be related to

the assumption of symmetric strain profile with respect to the centroidal axis of the sandwich
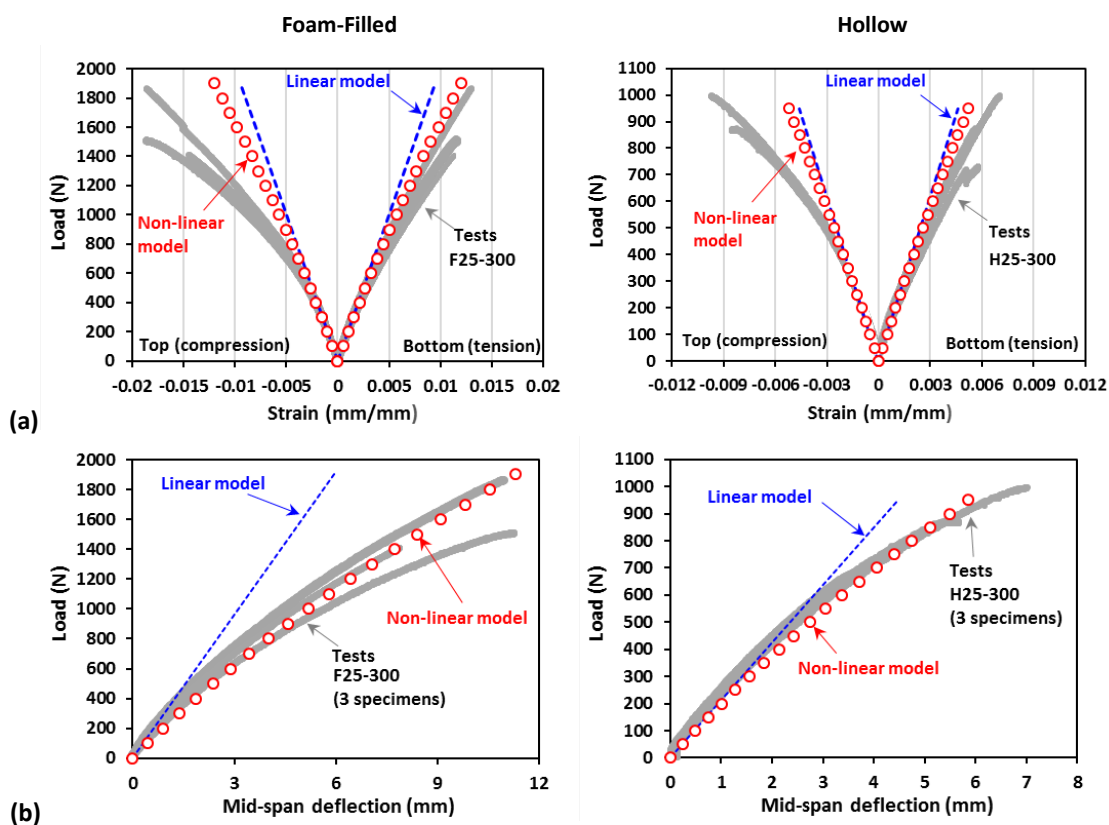
cross-section.

Figure 8. Perfomance of the analytical model predicting (a) load-strain and (b) load-

deflection of test specimens groups F25-300 and H25-300.

4.1.3. Discussions

Figure 9(a) shows the contribution of bending and shear in total deflection of the specimens F25-300 and H-25-300. It shows that both bending and shear deflections are non-linear. It also indicated that the bending contribution is more than shear contribution. Figure 9(b) shows the contribution percentage of the bending and shear deflection with respect the total deflection against as the mid-span deflection increases. The horizontal axis was normalized with respect to maximum deflection. The figure indicates that shear contribution increases as load increases. Also, shear contributes more in the hollow core than the foam-filled core, which is related to lower shear modulus of the hollow core. In average, the bending and contributes about 69% and 59% of the total deflection in F25-300 and H25-300, respectively. This means that the paper honeycomb cores (both foam-filled and hollow) used in this study were stiff enough to prevent large shear deformations violating the Euler-Bernoulli beam theory.
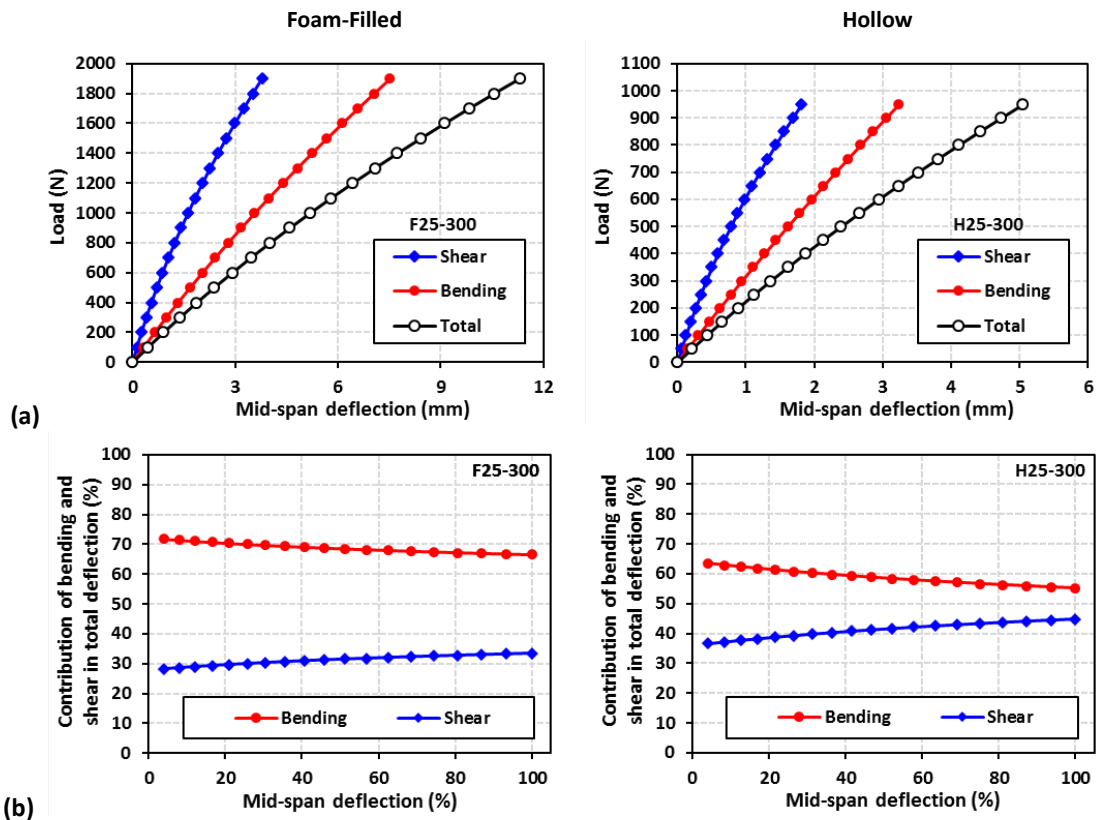
Figure 9. Contribution of bending and shear in total deflection of test specimens groups F25-300 and H25-300: (a) load vs. deflection and (b) persentage of contribution vs. percentage of maximum deflection.

It should be noted that sandwich composites with a soft core and stiff skins behave differently and they must be analyzed with a high-order sandwich composite theory [53][54][55] rather than the classical theories. The second author's group previously developed an analytical model [23] based on the non-proportional deformation of a soft core and stiff skins to determine the level of partial composite action due to a non-proportional strain distribution in the core and the skins. The model was applied to the sandwich beam specimens tested in this study and it was shown that if the shear modulus of the paper honeycomb was 0.96 MPa (instead of 19.6 MPa for the hollow core and 26.2 MPa for the foam-filled core), the degree of the partial composite action for the F25-300 and H25-300 specimens would be 95%. In order to achieve the same level of the partial composite action (i.e. 95%), the shear modulus of the 12 mm and 6 mm thick cores must be 1.31 MPa and 1.76 MPa, respectively. As the shear modulus of the cores used in this study were well above theses limits, the authors are confident that the use of the Euler-Bernoulli beam theory is justified.

In the experimental study, only load, displacement, and normal strains were measured and reported. Normal stress in the skins and shear stress and strain in the core can be obtained based on the nonlinear analytical model at any given load. For example, at the average experimental peak load of 1600 kN for the F25-300 specimens, the normal stress and strain of the tensile skin at the mid-span are calculated 137 MPa and 0.010 mm/mm, respectively. The

corresponding shear stress and strain at shear span are calculated 0.55 MPa and 0.024 mm/mm. The calculation can be done for other specimens and implemented in a parametric study for a broad range of geometrical and materials parameters.

4.2. Peak Load

In order to calculate the peak load of each specimen identifying the peak point of the load-strain and load-deflection curves obtained from the non-linear analytical model, three major failure modes are considered for the foam-filled specimens, namely: core shear, tensile rupture, and wrinkling failures. For the hollow core specimens, in addition to the wrinkling failure of the compressive skin, the dimpling or local buckling of the compressive skin surrounded with the hollow hexagonal core cell is also considered. The peak load of each specimen corresponding to each failure mode was calculated by the following equations obtained from the literature [56][57]:

$$P_{CS} = \frac{2\tau_c bc}{\sqrt{(\frac{aE_c}{2tE_f})^2 + 1}} \tag{10}$$

$$P_{TR} = \sigma_{fu}\frac{2btd}{a} \tag{11}$$

$$P_{WR} = 0.56E_f^{1/3}E_c^{2/3}\frac{2btd}{a} \tag{12}$$

$$P_{DM} = \frac{2E_f}{1 - v_f^2}\left(\frac{t}{s}\right)^2\frac{2btd}{a} \tag{13}$$

where P_{CS} is the core shear (CS) failure load, P_{TR} is the skin tension rupture (TR) failure load, P_{WR} is the skin wrinkling (WR) failure load, and P_{DM} is the skin dimpling (DM) failure load. In addition, b is the width of sandwich specimen, c is the core thickness, t is the skin thickness,

d is the distance between the skins' centers, a is shear span, and *s* is the size of the core cell in the direction of the skin's compressive stress. Also, E_f is the initial elastic modulus of skin, E_c is the initial elastic modulus of core, σ_{fu} is the tensile strength of skin, τ_c is the shear strength of core, and v_f is the initial Poisson's ratio of skin. The minimum value of the loads calculated from the equations is taken as the peak load. The theoretical peak load and actual peak load obtained from the experimental program are compared in Figure 10.
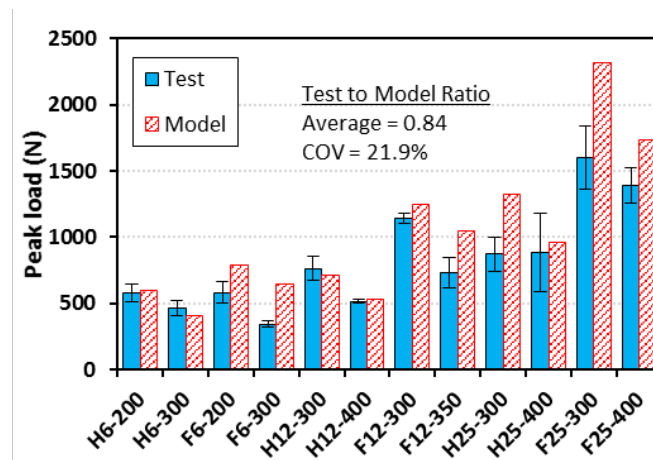

Figure 10. Comparison of peak load of model and test.

The error bars show one standard deviation above and below the average experimental value based on three identical specimens. The theoretical peak load of each group was obtained based on the average dimensions of three identical specimens. For specimens with the same type of core, higher peak loads were obtained along with the thicker core applied, and the model and test results were concordant with each other. For the comparison between the specimens with the same thickness of the cores, the model calculation results show that the peak loads of the foam-filled core specimens were higher than that of the hollow core specimens. The test to model ratio of each group was also calculated with an average value of

0.84 indicating the model over-predicted the peak load of the test specimens. It should be highlighted that the peak load equations were obtained from the literature and this study does not propose new equations. The overprediction of the peak load might be related to the complicated behavior of the honeycomb cells interaction with the filling foam and non-linear flax FRP skins. As the peak load equations were initially developed for conventional skin materials such as metallic and synthetic composite materials, the equations might need to be modified after an advanced simulation of the system in the future.

4.3. Initial Stiffness

The initial flexural stiffness K was also calculated based on Equation (1) considering both bending and shear deformations. The theoretical initial flexural stiffness D was calculated by Equation (7), and the theoretical initial shear stiffness U was calculated by Equation (9). The theoretical flexural stiffness K are compared with experimental values in Figure 11. As shown, the specimens gained higher initial stiffness when thicker core was applied. For comparison between the specimens with the same thickness of core, the difference between their initial stiffness were not obviously observed. Besides, it can be observed that the model calculation usually underestimated the initial stiffness of specimens slightly. The test to model ratio of each group was also calculated with an average value of 1.02 indicating the model slightly under-predicted the initial stiffness of the test specimens. The slight underprediction of stiffness by the model might be related to the shear modulus of the core materials. It is recommended to implement an advanced simulation for the paper honeycomb cores to have a better understanding of their shear behavior.
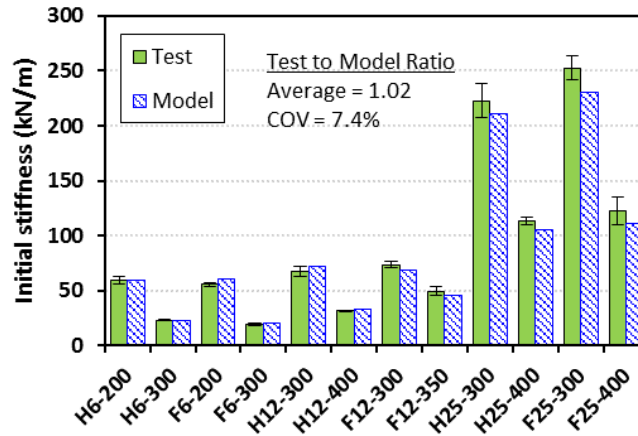
Figure 11. Comparison of initial stiffness of model and test.

4.4. Parametric Study

In this section, the effects of the flax FRP skin thickness and the core thickness, and the span length of sandwich beams with the width of 50 mm under three-point bending are evaluated using the non-linear analytical model presented and verified earlier. A case ID of FX-Y-LZ was used to note the core thickness as "X", the span length as "Y", and number of skin layers as "Z". In all cases, a foam-filled paper honeycomb was used as it showed higher strength than its hollow counterpart. Also, all cases were loaded under three-point bending.

4.4.1. Effect of Flax FRP Skin Thickness

The range of the skin thickness studied was 0.5, 1.0, 1.5, and 2.0 mm, representing 1, 2, 3, and 4 layers of unidirectional flax FRP layers per skin. This range was selected to cover a broad, yet practical range of possible layers of sandwich beams with the foam-filled paper honeycomb core thickness of 25 mm, beam width of 50 mm, and span length of 500 mm under three-point bending. The non-linear analytical model was applied to all four cases to obtain the variation load against bending, shear, and total deflection of the beams at mid-span as shown in Figure

12. Also, the failure mode of each case along with corresponding peak load was identified and noted on each diagram in Figure 12. It can be observed that as the thickness of the skins increased, the load capacity increased and failure mode was switched from tension rupture of skin to shear failure of the core. Also, the contribution of shear in total deformation increased from an average 17% to an average 50%, as the thickness of the skins increased.
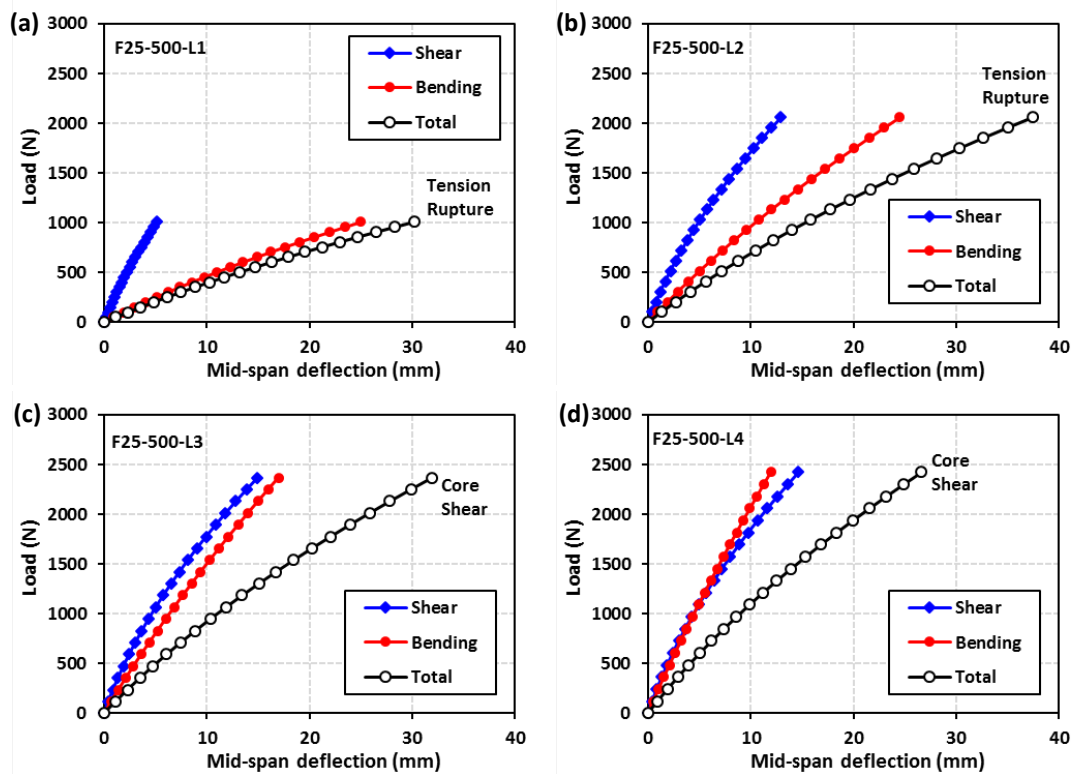

Figure 12. Effect of flax FRP skin thickness on the behavior of foam-filled paper honeycomb sandwich beams with (a) one layer, (b) two layers, (c) three layers, and (d) four layers of flax FRP per skin (three-point bending, c=25 mm, b=50 mm, S=500 mm).

4.4.2. Effect of Honeycomb Core Thickness

The range of the core thickness studied was 25, 50, 75, and 100 mm. This range was selected to cover a broad range of possible sandwich panel thicknesses from applicable ranges of doors

and furniture to walls. All four cases were considered with 2 layers of flax FRP layers per skin and beam width of 50 mm under three-point bending with 500 mm span. The results are shown in Figure 13. It is observed that as the core thickness increased from 25 to 100 mm, the load capacity increased and the ultimate deflection decreases, however the failure mode of tension rupture remained the same. Also, the contribution of shear in total bending increased from an average of 32% to an average of 65%, as the thickness of the core increased.
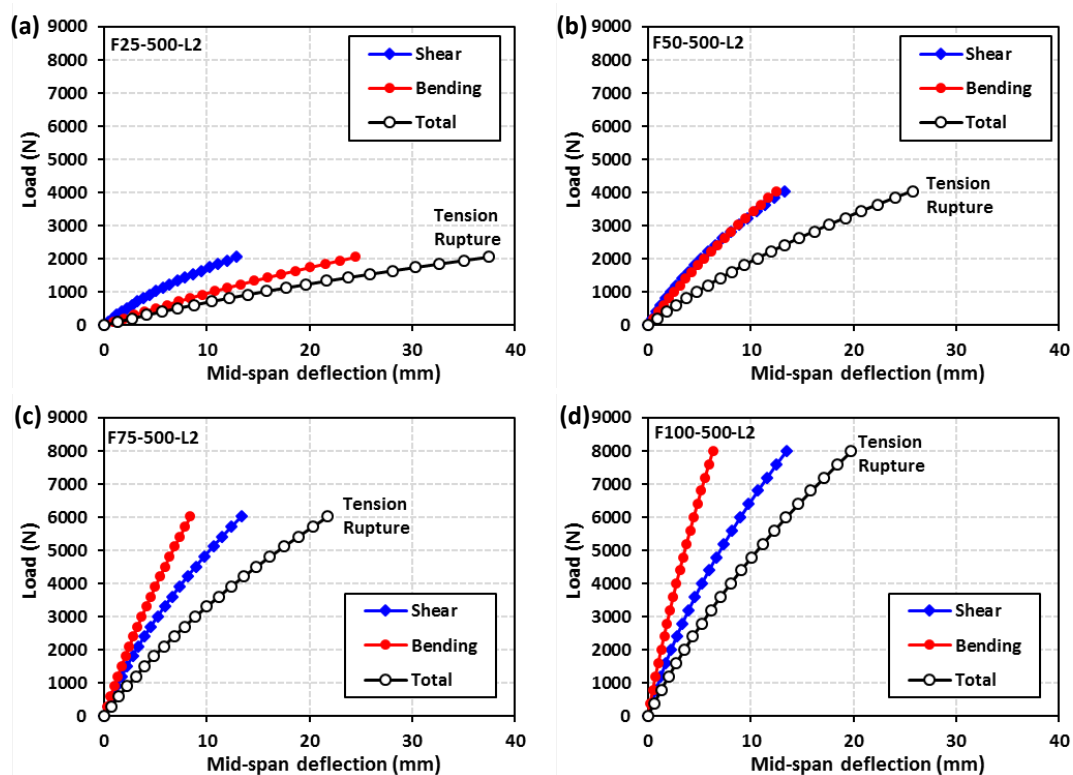

Figure 13. Effect of core thickness on the behavior of foam-filled paper honeycomb sandwich beams with the core thickness of (a) 25 mm, (b) 50 mm, (c) 75 mm, and (d) 100 mm (three-point bending, two layers of flax FRP per skin, b=50 mm, S=500 mm).

4.4.3. Effect of Span Length

Figure 14 shows the effect of span length changing from 200 mm to 500 mm with an interval

of 100 mm. All cases were considered with 2 layers of flax FRP layers per skin, core thickness of 25 mm, and beam width of 50 mm under three-point bending. As the span decreased from 500 mm to 200 mm, the contribution of shear in total deflection increased, however the beams became stronger and stiffer as expected and the mode of failure was changed from tensile rupture to core shear failure. It can be concluded that the non-linear contribution of the shear and bending in total deflection is a function of multiple geometrical parameters, however it can be engineered to achieve a desirable strength and stiffness.
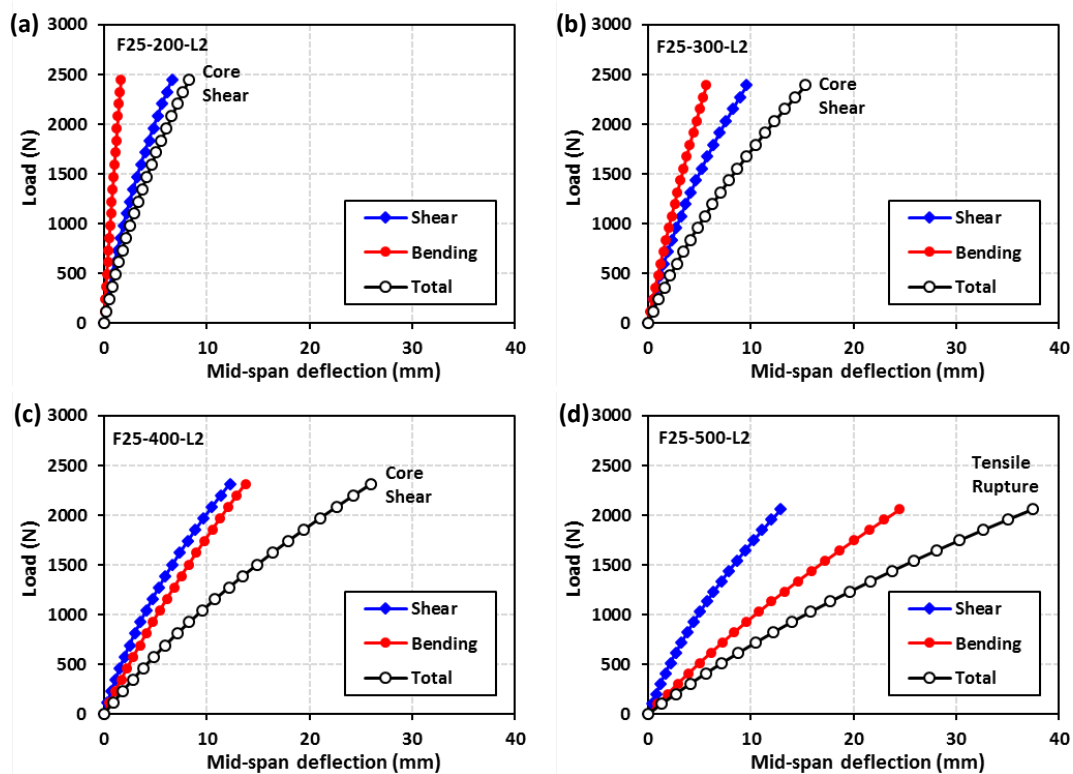

Figure 14. Effect of span length on the behavior of foam-filled paper honeycomb sandwich beams with the span of (a) 200 mm, (b) 300 mm, (c) 400 mm, and (d) 500 mm (three-point bending, two layers of flax FRP per skin, b=50 mm, c=25 mm).

5. FUTURE STUDIES AND APPLICATIONS

Limited number of small-scale specimens were tested in this study under one-way static

loading. Future studies may include testing more specimens to have a better confidence in terms of mode of failure. Also, large-scale panels made of bidirectional flax fabrics for the skins to be tested under two-way bending considering the effect of the bending and shear in a three-dimensional space. Moreover, the behavior of the bio-based sandwich panels needs to be studies under long-term loading to consider the creep effect of the bio-based components. Considering the effect of impact and cyclic loadings is also recommended to understand the dynamic and fatigue behavior of the system. Using bio-based foams to fill the cells of the paper honeycomb core is also encouraged to increase the bio content of the sandwich panels. Implementing advanced simulations is also recommended to have more in-depth understanding of the non-linearity of the bio-based skins interaction with paper honeycomb cores.

In terms of applications, the simplicity of the manufacturing process of paper honeycombs and can support mass production of the sandwich system for a variety of building and construction applications. The sustainability of products made of natural fibers can encourage more building applications to receive higher LEED (Leadership in Energy and Environmental Design) rating for green buildings. The bio-based sandwich panels studied in this research have many potentials to be used as walls, floors, and roofs in buildings, however more in-depth research is needed to understand the long-term performance of the materials. Until the availability of enough evidence verifying required long-term performance, the bio-based panels might be considered for less sensitive applications for non-structural and semi-structural components such as interior walls, doors, furniture, etc. in buildings considering required fire safety requirements.

6. CONCLUSIONS

The focus of this study was on the experimental behavior of sandwich composites made of bio-based components (i.e. flax FRP skins and paper honeycomb cores). The failure modes, load-deflection behavior, load-strain behavior, and moment-curvature behavior of the sandwich beam specimens were studied to evaluate the mechanical behavior of the sandwich composites. The flexural and shear stiffness of the specimens were obtained based on the moment-curvature and an ASTM method. The effect of the non-linearity of the skins and core on the behavior of the sandwich specimens was also evaluated. A non-linear analytical model was developed to predict the load-strain and load-deflection behavior of the test specimens. After verification, a parametric study was conducted to evaluate the effects of different geometrical parameters on the behavior of the bio-based sandwich composites. The following conclusion can be found:

- Majority of the specimens with hollow honeycomb cores were prematurely failed due to the local buckling of the compression skin. However, foam-filled core specimens were able to sustain higher loads achieving material failures such as skin tension rupture and core shear failure. By using the foam-filled cores instead of the hollow cores, the load capacity of the specimens with 12- and 25-mm thick core and span of 300 mm increased 49% and 83%, however it did not change the load capacity of 6-m thick cores. The foam filling did not affect the bending stiffness of the specimens with identical core thickness.

- Filling the paper honeycomb cells with the foam increased the bulk density of the cores from 40 kg/m^3 to 114 kg/m^3. In return, it increased the shear modulus of the cores from an average of 19.6 MPa to 26.2 MPa. Moreover, it significantly changed the failure mode and

load capacity of majority of the specimens based on the lateral support provided by the filling foam for the core cells and compressive skin.

- The load-deflection and load strain diagrams of the test specimens showed a non-linear behavior due to the non-linearity of flax FRP skins in tension and compression plus the nonlinearity of the paper honeycomb cores under shear.

- An analytical non-linear model based on the non-linearity of both the skins and the core was developed to predict the load-strain and load-deflection behavior of the test specimens. The model predicted the non-linear behavior of the test specimens with a relatively good agreement. The model needs to be refined to mimic the behavior of the compressive skin more accurately.

- A parametric study was performed on different geometrical parameters of the sandwich beams. It was shown that the thickness of both the core and skins can be engineered to achieve desirable strength and stiffness.

- Future studies may include large-scale sandwich panels made of bidirectional flax fabrics to be tested under two-way bending under short- and long-term loadings to evaluate the impact, dynamic, fatigue, and durability of the bio-based sandwich panels.

7. ACKNOWLEDGEMENTS

processing.

8. REFERENCE

[1] Hazizan, M. A., & Cantwell, W. J. (2003). The low velocity impact response of an aluminium honeycomb sandwich structure. Composites Part B: Engineering, 34(8), 679-687.

[2] Foo, C. C., Chai, G. B., & Seah, L. K. (2006). Quasi-static and low-velocity impact failure of aluminium honeycomb sandwich panels. Proceedings of the Institution of Mechanical Engineers, Part L: Journal of Materials: Design and Applications, 220(2), 53-66.

[3] Crupi, V., Kara, E., Epasto, G., Guglielmino, E., & Aykul, H. (2018). Theoretical and experimental analysis for the impact response of glass fibre reinforced aluminium honeycomb sandwiches. Journal of Sandwich Structures & Materials, 20(1), 42-69.

[4] He, W., Yao, L., Meng, X., Sun, G., Xie, D., & Liu, J. (2019). Effect of structural parameters on low-velocity impact behavior of aluminum honeycomb sandwich structures with CFRP face sheets. Thin-Walled Structures, 137, 411-432.

[5] Sun, G., Zhang, J., Li, S., Fang, J., Wang, E., & Li, Q. (2019). Dynamic response of sandwich panel with hierarchical honeycomb cores subject to blast loading. Thin-Walled Structures, 142, 499-515.

[6] Zinno, A., Prota, A., Di Maio, E., and Bakis, C. E. (2011). Experimental characterization of phenolic-impregnated honeycomb sandwich structures for transportation vehicles. Composite structures, 93(11), 2910-2924.

[7] Bakis, C.E., Bank, L.C., Brown, V., Cosenza, E., Davalos, J.F., Lesko, J.J., Machida, A.,

Rizkalla, S.H. and Triantafillou, T.C. (2002). Fiber-reinforced polymer composites for construction—State-of-the-art review. Journal of composites for construction, 6(2), 73-87.

[8] Manalo, A., Aravinthan, T., Fam, A., and Bemokrane, B. (2017). State-of-the-art review on FRP sandwich systems for lightweight civil infrastructure. Journal of Composites for Construction, 21(1), 04016068.

[9] Shan, C., and Yi, Y. (2017). An experimental and numerical study on the behavior of a continuous orthotropic bridge deck with sandwich construction. Thin-Walled Structures, 111, 138-144.

[10] Dweib, M. A., Hu, B., O'donnell, A., Shenton, H. W., and Wool, R. P. (2004). All natural composite sandwich beams for structural applications. Composite structures, 63(2), 147-157.

[11] Betts, D., Sadeghian, P. (2018). Experimental Behavior and Design-Oriented Analysis of Sandwich Beams with Bio-based Composite Facings and Foam Cores. Journal of Composites for construction, 22(4), 04018020.

[12] CoDyre, L., Mak, K., and Fam, A. (2018). Flexural and axial behaviour of sandwich panels with bio-based flax fibre-reinforced polymer skins and various foam core densities. Journal of Sandwich Structures and Materials, 20(5), 595-616.

[13] Wroblewski, L., Hristozov, D., and Sadeghian, P. (2016). Durability of bond between concrete beams and FRP composites made of flax and glass fibers. Construction and Building Materials, 126, 800-811.

[14] Shah, D. U., Schubel, P. J., and Clifford, M. J. (2013). Can flax replace E-glass in structural

composites? A small wind turbine blade case study. Composites Part B: Engineering, 52, 172-181.

[15] Baiardo, M., Zini, E., and Scandola, M. (2004). Flax fibre–polyester composites. Composites Part A: Applied Science and Manufacturing, 35(6), 703-710.

[16] Mohanty, A.K., Misra, M., and Drzal, L.T. (2002). Sustainable bio-composites from renewable resources: opportunities and challenges in the green materials world. Journal of Polymers and the Environment, 10(1-2), 19-26.

[17] Liu, Z., Erhan, S.Z., Akin, D.E., and Barton, F.E. (2006). "Green" composites from renewable resources: preparation of epoxidized soybean oil and flax fiber composites. Journal of agricultural and food chemistry, 54(6), 2134-2137.

[18] Fam, A., Eldridge, A., and Misra, M. (2014). Mechanical characteristics of glass fibre reinforced polymer made of furfuryl alcohol bio-resin. Materials and structures, 47(7), 1195-1204.

[19] Belingardi, G., Cavatorta, M.P., and Duella, R. (2003). Material characterization of a composite–foam sandwich for the front structure of a high speed train. Composite structures, 61(1-2), 13-25.

[20] Fam, A., and Sharaf, T. (2010). Flexural performance of sandwich panels comprising polyurethane core and GFRP skins and ribs of various configurations. Composite Structures, 92(12), 2927-2935.

[21] Dharmasena, K. P., Wadley, H. N., Xue, Z., & Hutchinson, J. W. (2008). Mechanical response of metallic honeycomb sandwich panel structures to high-intensity dynamic

loading. International Journal of Impact Engineering, 35(9), 1063-1074.

[22] Aktay, L., Johnson, A. F., and Kröplin, B. H. (2008). Numerical modelling of honeycomb core crush behaviour. Engineering Fracture Mechanics, 75(9), 2616-2630.

[23] McCracken, A., and Sadeghian, P. (2018). Partial-composite behavior of sandwich beams composed of fiberglass facesheets and woven fabric core. Thin-Walled Structures, 131, 805-815.

[24] Ude, A. U., Ariffin, A. K., and Azhari, C. H. (2013). Impact damage characteristics in reinforced woven natural silk/epoxy composite face-sheet and sandwich foam, coremat and honeycomb materials. International Journal of Impact Engineering, 58, 31-38.

[25] Feraboli, P., and Masini, A. (2004). Development of carbon/epoxy structural components for a high performance vehicle. Composites Part B: Engineering, 35(4), 323-330.

[26] Sadeghian, P., Hristozov, D, and Wroblewski, L. (2016). Experimental and analytical behavior of sandwich composite beams: Comparison of natural and synthetic materials. Journal of Sandwich Structures and Materials. Journal of Sandwich Structure and Materials, 20(3), 287 – 307.

[27] Dong, Dahai, Qingguo, and Shaoqing. (2014). An approach on identification of equivalent properties of honeycomb core using experimental modal data. Finite Elements in Analysis and Design, 90(C), 84-92

[28] Vaidya, U., Kamath, M., Mahfuz, H., and Jeelani, S. (1998). Low Velocity Impact Response of Resin Infusion Molded Foam Filled Honeycomb Sandwich Composites. Journal of Reinforced Plastics and Composites, 17(9), 819-849.

[29] Burlayenko, V. N., and Sadowski, T. (2009). Analysis of structural performance of sandwich plates with foam-filled aluminum hexagonal honeycomb core. Computational Materials Science, 45(3), 658-662.

[30] Mozafari, H., Khatami, S., Molatefi, H., Crupi, V., Epasto, G., and Guglielmino, E. (2016). Finite element analysis of foam-filled honeycomb structures under impact loading and crashworthiness design. International journal of crashworthiness, 21(2), 148-160.

[31] Zhang, P., Cheng, Y., Liu, J., Li, Y., Zhang, C., Hou, H., & Wang, C. (2016). Experimental study on the dynamic response of foam-filled corrugated core sandwich panels subjected to air blast loading. Composites Part B: Engineering, 105, 67-81.

[32] Zhang, Y., Liu, Q., He, Z., Zong, Z., & Fang, J. (2019). Dynamic impact response of aluminum honeycombs filled with Expanded Polypropylene foam. Composites Part B: Engineering, 156, 17-27.

[33] Jayaram, R. S., Nagarajan, V. A., & Vinod Kumar, K. P. (2019). Compression and low velocity impact response of sandwich panels with polyester pin-reinforced foam filled honeycomb core. Journal of Sandwich Structures & Materials, 21(6), 2014-2030.

[34] Wang, D. (2009). Impact behavior and energy absorption of paper honeycomb sandwich panels. International Journal of Impact Engineering, 36(1), 110-114.

[35] Dongmei, W. (2009). Cushioning properties of multi-layer corrugated sandwich structures. Journal of Sandwich Structures and Materials, 11(1), 57-66.

[36] Chen, Z., and Yan, N. (2012). Investigation of elastic moduli of Kraft paper honeycomb core sandwich panels. Composites Part B: Engineering, 43(5), 2107-2114.

[37] Sypeck, D. J. (2005). Cellular truss core sandwich structures. Applied Composite Materials, 12(3-4), 229-246.

[38] Aboura, Z., Talbi, N., Allaoui, S., and Benzeggagh, M. L. (2004). Elastic behavior of corrugated cardboard: experiments and modeling. Composite structures, 63(1), 53-62.

[39] McCracken, A., and Sadeghian, P. (2018). Corrugated cardboard core sandwich beams with bio-based flax fiber composite skins. Journal of Building Engineering, 20, 114-122.

[40] Betts, D., Sadeghian, P., & Fam, A. (2020). Structural Behavior of Sandwich Beams with Flax Fiber–Reinforced Polymer Faces and Cardboard Cores under Monotonic and Impact Loads. Journal of Architectural Engineering, 26(2), 04020013.

[41] Wang, D. M., Wang, Z. W., and Liao, Q. H. (2009). Energy absorption diagrams of paper honeycomb sandwich structures. Packaging Technology and Science: An International Journal, 22(2), 63-67.

[42] Castro, O., Silva, J. M., Devezas, T., Silva, A., & Gil, L. (2010). Cork agglomerates as an ideal core material in lightweight structures. Materials & Design, 31(1), 425-432.

[43] Lakreb, N., Bezzazi, B., and Pereira, H. (2015). Mechanical behavior of multilayered sandwich panels of wood veneer and a core of cork agglomerates. Materials and Design (1980-2015), 65, 627-636.

[44] Walsh, J., Kim, H. I., and Suhr, J. (2017). Low velocity impact resistance and energy absorption of environmentally friendly expanded cork core-carbon fiber sandwich composites. Composites Part A: Applied Science and Manufacturing, 101, 290-296.

[45] Dweib, M. A., Hu, B., O'donnell, A., Shenton, H. W., and Wool, R. P. (2004). All natural

composite sandwich beams for structural applications. Composite structures, 63(2), 147-157.

[46] Stocchi, A., Colabella, L., Cisilino, A., and Álvarez, V. (2014). Manufacturing and testing of a sandwich panel honeycomb core reinforced with natural-fiber fabrics. Materials and Design, 55, 394-403.

[47] Du, Y., Yan, N., and Kortschot, M. T. (2013). An experimental study of creep behavior of lightweight natural fiber-reinforced polymer composite/honeycomb core sandwich panels. Composite Structures, 106, 160-166.

[48] Mak, K., Fam, A., and MacDougall, C. (2015). Flexural behavior of sandwich panels with bio-FRP skins made of flax fibers and epoxidized pine-oil resin. Journal of Composites for Construction, 19(6), 04015005.

[49] Betts D, Sadeghian P, Fam A. Tensile Properties of Flax FRP Composites. In 6th Asia-Pacific Conference on FRP in Structures (APFIS 2017) 2017 Jul 19. 6th Asia-Pacific Conference on FRP in Structures, Singapore.

[50] Palomba, G., Crupi, V., & Epasto, G. (2019). Collapse modes of aluminium honeycomb sandwich structures under fatigue bending loading. Thin-Walled Structures, 145, 106363.

[51] ASTM D7250. Standard practice for determining sandwich beam flexural and shear stiffness. West Conshohocken, PA, USA.

[52] Betts, D., Sadeghian, P. and Fam, A. (2019). "Experiments and analysis of the impact behavior of sandwich panels constructed with flax fibre-reinforced polymer faces and foam cores." Journal of Sandwich Structures and Materials, SAGE, DOI:

https://doi.org/10.1177/1099636220925073.

[53] Frostig, Y., Baruch, M., Vilnay, O., and Sheinman, I. (1992). High-order theory for sandwich-beam behavior with transversely flexible core. Journal of Engineering Mechanics, 118(5), 1026-1043.

[54] Salami, S. J., Sadighi, M., and Shakeri, M. (2015). Improved high order analysis of sandwich beams by considering a bilinear elasto-plastic behavior of core: an analytical and experimental investigation. International Journal of Mechanical Sciences, 93, 270-289.

[55] Sokolinsky, V. S., Shen, H., Vaikhanski, L., & Nutt, S. R. (2003). Experimental and analytical study of nonlinear bending response of sandwich beams. Composite Structures, 60(2), 219-229.

[56] Triantafillou, T.C. and Gibson, L.J. (1987). Failure mode maps for foam-core sandwich beams. U.S. Army Construction Engineering Research Lab.

[57] Ley, R.P., Lin, W. and Mbanefo, U. (1999). Facesheet Wrinkling in Sandwich Structures. Northrop Grumman Corporation, El Segundo, California, USA.